

Accounts

Dynamics of Molecules and Clusters Studied by Low-Temperature Matrix-Isolation Infrared Spectroscopy and Density-Functional-Theory Calculations

Munetaka Nakata

Graduate School of BASE (Bio-Applications and Systems Engineering), Tokyo University of Agriculture and Technology, Koganei, Tokyo 184-8588

(Received October 9, 2001)

This article presents an account of applications of low-temperature matrix-isolation (MI) infrared spectroscopy combined with density-functional-theory (DFT) calculations to studies of dynamics of molecules and clusters. The MI technique using a conventional Fourier transform infrared (FTIR) spectrophotometer can measure infrared spectra of less stable isomers, clusters produced by photolysis or supersonic-jet expansion, electronically excited species, and unstable radicals. The observed wavenumbers are compared with the calculated values obtained by the DFT calculation and are used for accurate identification of the structures, including conformations around some rotational axes. Thus photoreaction mechanisms of molecules and clusters are elucidated.

Almost half a century has passed since the low-temperature rare-gas matrix-isolation technique (MI) was proposed by Pimentel et al.[1,2] From this first step to the present day, this technique has been developed by combinations with various spectroscopies such as infrared, Raman, absorption, Mösbauer, photoelectron, NMR, and ESR.[3–5] The number of published papers is beyond 150 every year.[6,7] The matrix-isolation infrared spectroscopy is one of the most powerful techniques to study structures of unstable species produced by UV irradiation, electron impact, discharge, and high-temperature heating.

The development of quantum chemical calculation has accelerated the use of this technique to identify unknown species. For example, the calculated vibrational wavenumbers obtained by the density-functional-theory (DFT) method[8,9] satisfactorily reproduce the experimental data obtained by MI within 10 cm^{-1} even for radical species, if a suitable scaling factor is used. This fact provides a more powerful technique to examine the dynamics of molecules and clusters in photochemistry. In this article brief explanations about MI and DFT are given in the beginning; then recent results for photo-induced dynamics of molecules and clusters in low-temperature rare-gas matrices are shown; from such results the usefulness of this new combination of MI with DFT is found.

1. Low-Temperature Matrix-Isolation Infrared Spectroscopy

MI is a method in which sample gases are diluted with rare gases such as argon, krypton, xenon and then the premixed gases are frozen on a substrate at low temperature in vacuum. Since molecules isolated in inactive rare-gas matrices are chemically and physically stabilized, it is possible to measure infrared spectra of unstable species such as radicals, reaction intermediates, and electronically excited species with a conventional FTIR spectrophotometer. Neither excess thermal reaction nor intermolecular reaction takes place in the low-temperature matrices. Furthermore, infrared spectra of species isolated in low-temperature matrices have some excellent characteristic features. For example, bandwidths are rather sharp because of no distribution of rotational-energy levels, i.e.; molecules are in principle populated at the lowest rotational-energy level. Another feature is that band positions are nearly equal to those measured in the gas phase, because there is neither intermolecular interaction in liquid and solid nor interaction with solvents in solution. Then, MI provides ideal experimental information on molecules and clusters to be compared with theoretical information obtained by quantum chemical calculations.

2. Density-Functional-Theory Calculation

There are some theoretical methods to treat the interaction of electrons contained in a molecule. The configuration-interaction (CI) method explicitly considers contributions of electronically excited states. For example, MP2 (Møller–Plesset) and MP4 methods consider electron interaction by the second and fourth perturbation theory, respectively.[10] On the other hand, electron density can be expressed in terms of suitable functionals in the density-functional-theory (DFT) calculation. This method is based on the theory of Kohn and Hohenberg,[11]

who proposed a potential function defining electron density of an electron system uniquely, where a theorem saying that the approximate energy corresponding to the electron density is always higher than the true one was used. Kohn and Sham[12] found that the function of electron density could be expressed as the sum of the squares of the absolute values of one-electron wave functions determined by the Kohn–Sham equation.

Now the DFT method is known to be one of the most useful molecular orbital calculations to predict vibrational wavenumbers and geometrical structures.[13,14] Especially the B3LYP method, which combines Becke's three-parameter hybrid functional[15] and the correlation functional of Lee, Yang and Parr,[16] has been applied to several simple molecules; Wong[13] and Scott and Radom[14] independently compared the observed wavenumbers for 1066 vibrational modes for 122 molecules with the corresponding values calculated by the DFT/B3LYP/6-31G* method and insisted that the overall root-mean-square deviation, 34 cm^{-1}, was significantly smaller than that calculated by the MP2 method, 61 cm^{-1}.

3. Identification of Dewar Pyridine and Picolines

Dewar benzene has been extensively studied in the fields of organic and physical chemistry since Dewar proposed it in 1866.[17] This compound was first synthesized by Ward and Winshnok in 1968.[18] The geometrical structure was determined by vibrational spectroscopy,[19,20] gas electron diffraction,[21] and microwave spectroscopy[22] in the 1970s. On the other hand, only a few studies of Dewar pyridine had been published until our studies began to appear.[23,24] Dewar pyridine seems to be rather less stable than Dewar benzene. We measured and identified infrared bands of Dewar pyridine and methyl-substituted pyridines (picolines) by a combination of the MI technique with the DFT calculation.[25–28]

3.1 Dewar Pyridine. Unlike Dewar benzene, two isomers can be considered for Dewar pyridine, as shown in Scheme 1. Isomer I has a C–C bridging bond and has no symmetry element, whereas Isomer II has a C–N bridging bond and has a symmetry plane. In order to determine which isomer is more stable, we performed DFT calculations using the GAUSSIAN 94 program[29] with the B3LYP/6-31++G** to optimize the geometrical structures.[25] The obtained geometrical structures are illustrated in Fig. 1, where the length of the C–N bridging bond for Isomer II, 1.536 Å, is shorter than that of the C–C bridging bond for Isomer I, 1.564 Å. This finding implies that Isomer II is more strained than Isomer I. Indeed, the relative energy of Isomer I is lower by 38 kJ mol^{-1} than Isomer II.[30,31] Then, it should be possible that Isomer I exists in low-temperature argon matrices.

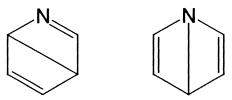

Scheme 1.

In order to measure infrared spectra of Dewar pyridine, the vapor of pyridine was premixed with argon gas and deposited on a CsI plate cooled at 15 K by a closed-cycle helium refrigeration unit. The matrix sample was exposed to the UV light introduced through a water filter to remove excess thermal reactions. A difference spectrum between the spectra measured before and after UV irradiation is shown in Fig. 2. The decreasing and increasing bands are due to pyridine and a photoproduct, respectively. In order to identify the photoproduct, we compared the calculated spectral patterns of Isomers I and II obtained by the DFT calculation in Fig. 2. The observed infrared spectrum is similar to the spectral pattern of Isomer I, although the strong bands around 850 and 750 cm^{-1} split into three peaks. These splits disappeared when xenon was used as a matrix gas instead of argon. Judging from the foregoing rel-

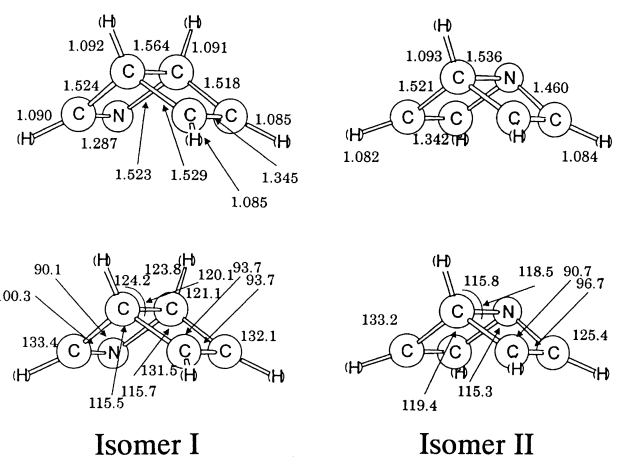

Fig. 1. Optimized geometrical structures of Dewar pyridine. Bond lengths and angles are given in Å and in degrees, respectively. (Transfer from *J. Photochem. Photobiol. A*: *Chem.*, **123**, 27 (1999)).

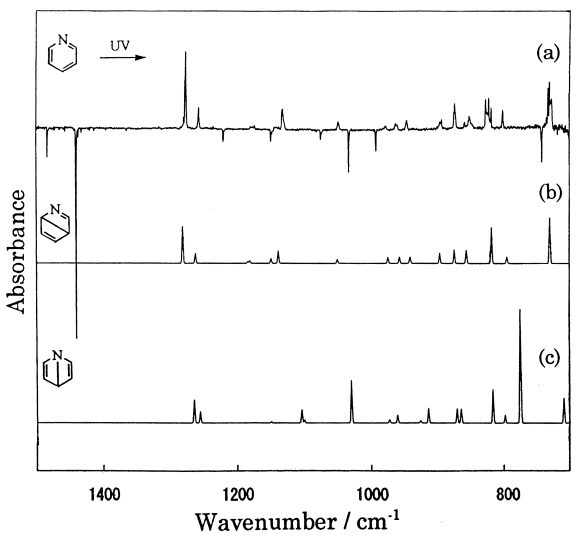

Fig. 2. Observed and calculated infrared spectra of Dewar pyridine. (a) A difference spectrum between those observed before and after 10-min UV irradiation. Spectral patterns of (b) Isomer I and (c) Isomer II estimated by DFT. (Transfer from *J. Photochem. Photobiol. A*: *Chem.*, **123**, 26 (1999)).

ative energy and the spectral patterns, we concluded that Isomer I of Dewar pyridine was selectively produced from pyridine in an argon matrix by UV irradiation. This conclusion was confirmed by the vibrational analysis of infrared bands of deuterated Dewar species.

3.2 Dewar Picolines. Similar experiments were performed for picolines, i.e., methyl-substituted pyridines.[26,27] In the case of 2-picoline, there are three possible isomers, as shown in Scheme 2. In order to determine the conformation of Dewar 2-picoline, the DFT calculations were performed. The energy differences from 2-picoline were calculated to be 307, 322, and 349 kJ mol^{-1} for Isomers I, II, and III, respectively.

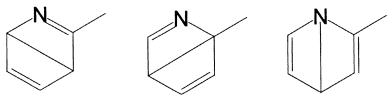

Scheme 2.

A difference spectrum between the spectra measured before and after UV irradiation is shown in Fig. 3. The decreasing and increasing bands were due to 2-picoline and a photoproduct, respectively. In order to identify the photoproduct, we compared the calculated spectral patterns of Isomers I, II, and III obtained by the DFT calculation in Fig. 3. The observed bands were assigned to Isomer I, which has a C–C bridging bond and an N=C–CH_3 group. No other isomer bands were observed, although the energy difference between Isomers I and II was calculated to be less than 15 kJ mol^{-1}.

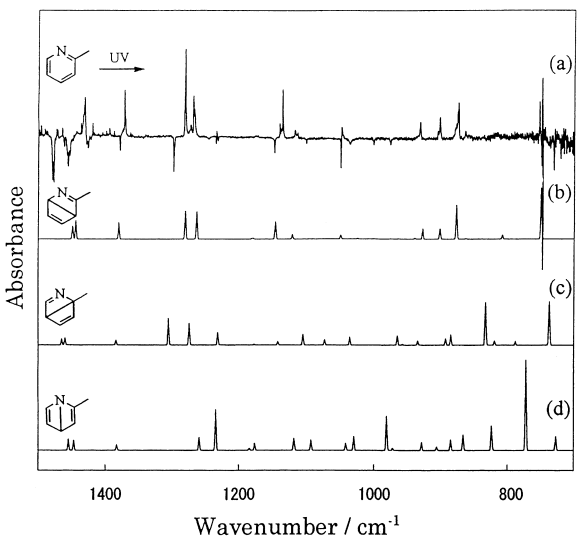

Fig. 3. Observed and calculated infrared spectra of Dewar 2-picoline. (a) A difference spectrum between those observed before and after 10-min UV irradiation. Spectral patterns of (b) Isomer I, (c) Isomer II, and (d) Isomer III estimated by DFT. (Transfer from *Chem. Phys. Lett.*, **308**, 404 (1999)).

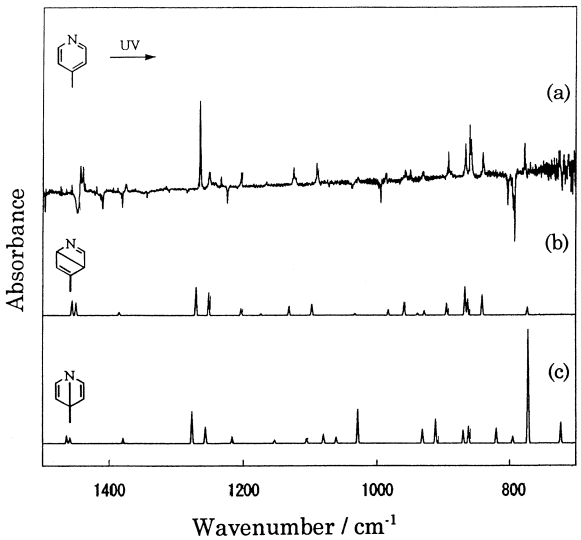

Fig. 4. Observed and calculated infrared spectra of Dewar 4-picoline. (a) A difference spectrum between those observed before and after 10-min UV irradiation. Spectral patterns of (b) Isomer I and (c) Isomer II estimated by DFT. (Transfer from *Chem. Phys. Lett.*, **322**, 365 (2000)).

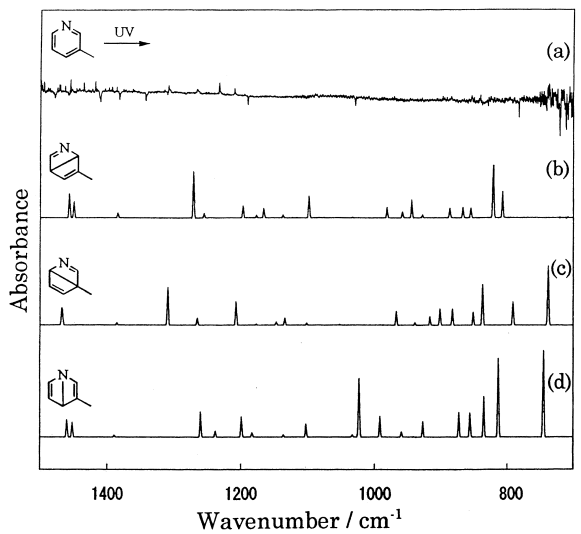

Fig. 5. Observed and calculated infrared spectra of Dewar 3-picoline. (a) A difference spectrum between those observed before and after 10-min UV irradiation. Spectral patterns of (b) Isomer I, (c) Isomer II, and (d) Isomer III estimated by DFT. (Unpublished data).

Similarly, the observed bands of Dewar 4-picoline were also compared with the calculated spectral patterns of two possible isomers, C–C bridging and C–N bridging isomers, in Fig. 4. The spectral pattern of the C–C bridging isomer reproduced the observed spectrum satisfactorily.

As shown in Fig. 5, the intensities of the photoproducts of 3-picoline were relatively weaker than those of the others. We also calculated the spectral patterns of three possible isomers, but none of them was consistent with the observed spectrum. It is known that reactivity on the *meta* position of pyridine is

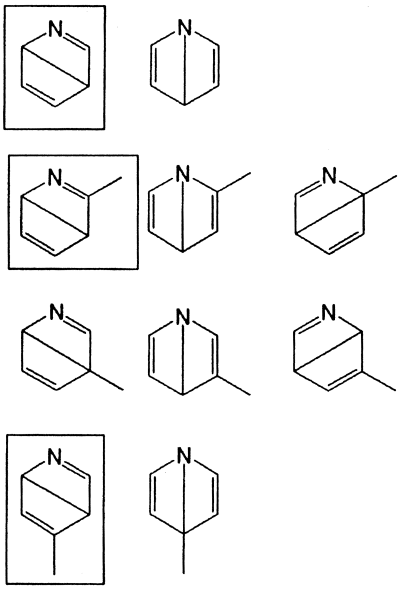

Fig. 6. Possible Dewar pyridine and picolines. Species detected by MI are marked with a square.

different from reactivities on the *ortho* and *para* positions. The present results on the production of Dewar picolines may be related to the reactivity.

Dewar species detected by our MI studies are marked with a square in Fig. 6.[28] No infrared bands of C–N bridging Dewar isomer nor of CH_3C–C bridging Dewar isomer were observed in pyridine and picolines.

4. van der Waals Clusters Produced by Photolysis in Argon Matrices

A cluster is defined as an assembly of a number of atoms or molecules. The properties of clusters are different from those of atoms, molecules, and bulk matters. Since clusters formed by van der Waals forces are easily broken and dissociated into atoms or molecules by a small amount of thermal energy, it is hard to study their structures and properties under normal experimental conditions. On the other hand, MI is a useful technique to study van der Waals clusters which are stabilized at low-temperature in an inactive cage of rare-gas atoms. We measured infrared spectra of van der Waals clusters of small molecules yielded by UV dissociation of molecules in a matrix cage with a conventional FTIR spectrophotometer. The observed infrared bands were compared with the corresponding calculated values and used to estimate their structures.[32–34]

4.1 HCN Clusters. When three carbon atoms of benzene are substituted by nitrogen atoms, the molecule is called triazine. Photoreaction mechanisms of 1,3,5-triazine were studied by photofragment translational spectroscopy.[35] It was reported that three HCN molecules were produced from 1,3,5-triazine in the gas phase, as shown in Scheme 3; naturally the photoproducts, HCN molecules, move freely. On the other hand, HCN molecules produced from 1,3,5-triazine in a low-temperature argon matrix should be constrained in an argon cage, where the most stable conformation is chosen.

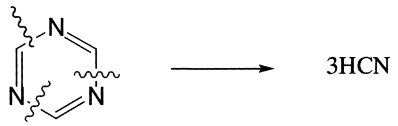

Scheme 3.

A matrix sample of 1,3,5-triazine/Ar was irradiated with UV light from a superhigh-pressure mercury lamp through a water filter. An infrared difference spectrum between the spectra measured before and after UV irradiation is shown in Fig. 7. Only one band was observed at 3264 cm^{-1} in the C–H stretching region. This means that the three HCN molecules dissociated from 1,3,5-triazine are located in an equivalent environment as cyclic $(HCN)_3$.[36] In the C≡N stretching region, only one band appeared at 2098 cm^{-1}, while the bands for in-plane and out-of-plane H–C≡N bending modes were observed at 764 and 736 cm^{-1}, respectively. So, we concluded that cyclic $(HCN)_3$ is the most stable conformer in argon matrices. The

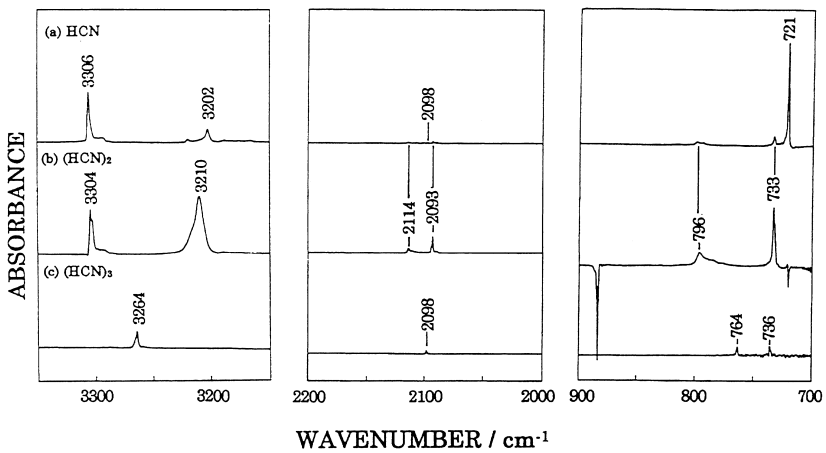

Fig. 7. Infrared spectra of HCN clusters in low-temperature argon matrices. (a) HCN/Ar = 1/1000. (b) Linear $(HCN)_2$ produced by photolysis of s-tetrazine. (c) Cyclic $(HCN)_3$ produced by photolysis of *s*-triazine. (Transfer from *J. Mol. Struct.*, **413/414**, 367 (1997)).

Table 1. Observed and Calculated Vibrational Wavenumbers of $(HCN)_n$ Clusters (in cm^{-1})

	C–H str.		C≡N str.		H–C≡N bend.		Comment
	Obsd	Calcd[a)]	Obsd	Calcd[a)]	Obsd	Calcd[a)]	
HCN	3306	3306	2098	2098	721	721[b)]	
$(HCN)_2$	3304	3303	2114	2111	733	728[b)]	HCN···
	3210	3219	2093	2088	796	850[b)]	···HCN
$(HCN)_3$	3264	3274	i.a.[c)]	2097	764	774	In-plane
	i.a.[c)]	3269	2098	2096	i.a.[c)]	768[b)]	In-plane
					i.a.[c)]	740	Out-of-plane
					736	736[b)]	Out-of-plane

a) Scaling factors are assumed so as to reproduce the observed wavenumbers of monomer. b) Degenerate mode. c) Infrared-inactive mode.

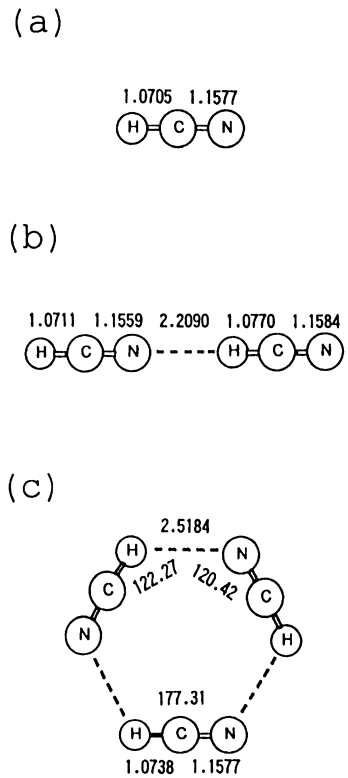

Fig. 8. Optimized geometrical structures of $(HCN)_n$ clusters. (a) HCN monomer. (b) Linear $(HCN)_2$. (c) Cyclic $(HCN)_3$. Bond lengths and angles are in Å and in degrees, respectively. (Transfer from *J. Mol. Struct.*, **413/414**, 368 (1997))

calculated wavenumbers were consistent with the corresponding observed values, if suitable scaling factors were used, as shown in Table 1. It was found that HCN molecules are slightly bent in the optimized geometry, as shown in Fig. 8.

Similarly, one N_2 and two HCN molecules are produced by photolysis of 1,2,4,5-tetrazine in the gas phase, as shown in Scheme 4.[37]

When a matrix sample of 1,2,4,5-tetrazine was irradiated by UV light, two HCN molecules produced in an argon matrix formed a linear dimer. A difference spectrum between the spectra measured before and after UV irradiation is shown in

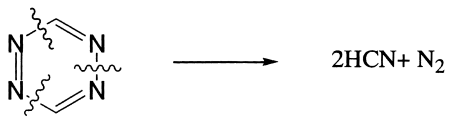

Scheme 4.

Fig. 7. Two C–H stretching bands were observed at 3304 and 3210 cm^{-1}. The higher wavenumber band was easily assigned to the free C–H stretching mode, because its wavenumber was almost identical with that of the monomer isolated in argon matrices. The lower-wavenumber band, which showed a shift of about 100 cm^{-1} from the HCN monomer band, was assigned to the hydrogen-bonding C–H stretching mode. The bandwidth was larger, probably because of the influence of the co-photoproduct N_2. The bands observed at 2114 and 2093 cm^{-1} were assigned to the hydrogen-bonding and free C–N stretching modes, respectively. The bands observed at 796 and 733 cm^{-1} bands were also assigned to the hydrogen bonded and free H–C–N bending modes, respectively. Thus we concluded that HCN dimer is linear. The optimized geometry is shown in Fig. 8, where the intermolecular distance between two HCN molecules was calculated to be 2.209 Å. The calculated wavenumbers were consistent with the corresponding values, as shown in Table 1.

4.2 HCN and HC≡CH Clusters. A similar experiment was performed for pyrimidine.[34] In this case, one HC≡CH and two HCN molecules may be produced from pyrimidine upon UV irradiation, as shown in Scheme 5.

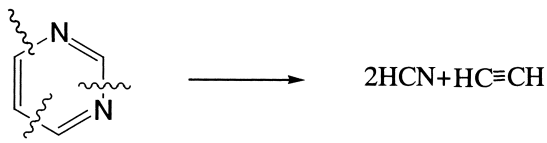

Scheme 5.

The DFT calculation resulted in two optimized structures for HC≡CH···$(HCN)_2$ clusters, as shown in Fig. 9. One is a linear cluster where one hydrogen atom of HC≡CH is bonded to the nitrogen atom of the linear HCN dimer. The other is a T-shaped cluster where one hydrogen atom of the linear HCN

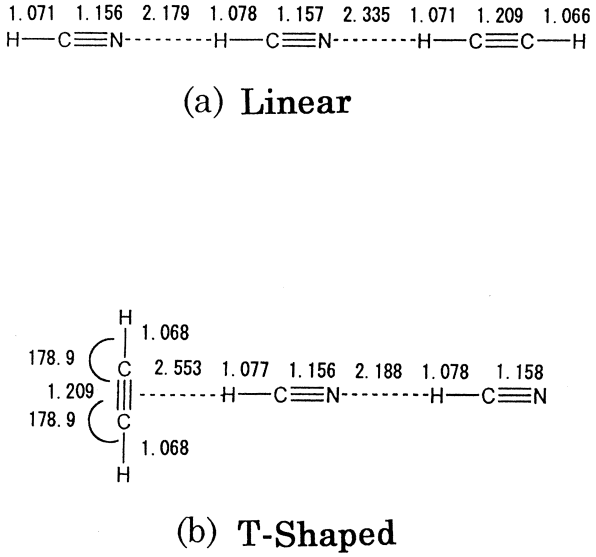

Fig. 9. Optimized geometrical structures of HC≡CH···$(HCN)_2$ clusters. (a) Linear cluster. (b) T-Shaped cluster. Bond lengths and angles are in Å and in degrees, respectively. (Unpublished data).

dimer is bonded to the π electrons of HC≡CH. The calculated relative energy of the linear cluster is lower than that of the T-shaped cluster, but the difference is only 1.3 kJ mol^{-1}. Then both clusters may co-exist in low-temperature argon matrices.

A difference spectrum of pyrmidine between the spectra measured before and after UV irradiation is shown in Fig. 10. In the C–H stretching region of HCN and HC≡CH, at least six peaks were observed. In the C≡N stretching region, one weak band was observed, while more than four peaks were observed in the skeleton-bending region. The observed wavenumbers are summarized and compared with the scaled calculated values in Table 2. It was easily found that the both linear and T-shaped clusters co-exist in low-temperature argon matrices.

5. van der Waals Clusters Produced by Supersonic-Jet Expansion

Supersonic-jet expansion is often used to cool a gas sample for application in a variety of problems in chemical physics.[38,39] For example, infrared spectra of van der Waals clusters produced by this technique have been observed by high-resolution high-sensitivity laser spectroscopy, although the spectral region observed is limited to one vibrational mode. If it is possible to isolate van der Waals clusters produced by supersonic-jet expansion in low-temperature argon matrices, their infrared spectra in the whole region can be easily and simultaneously measured with a conventional FTIR spectrophotometer. However, one may have the question as to whether or not van der Waals clusters are frozen on a cold substrate without dissocia-

Table 2. Observed and Calculated Vibrational Wavenumbers of HCCH···$(HCN)_2$ Clusters (cm^{-1})

Obsd	Calcd[a)]	Cluster[b)]	Mode
3315[c)]			
3293	3302	Linear	C–H str. of HCN
3284	3283	T-Shaped	C–H str. of HC≡CH
3255	3252	Linear	C–H str. of HC≡CH
3224	3225	T-Shaped	C–H str. of HCN
3208	3206	Linear	C–H str. of HCN
	3206	T-Shaped	C–H str. of HCN
2121	2112	Linear	C≡N str. of HCN
	2102	T-Shaped	C≡N str. of HCN
	2094	Linear	C≡N str. of HCN
	2087	T-Shaped	C≡N str. of HCN
870	869	Linear	bend. of HCN
855	857	T-Shaped	bend. of HCN
853	855	T-Shaped	bend. of HCN
	809	Linear	bend. of HC≡CH
	805	T-Shaped	bend. of HCN
	789	T-Shaped	bend. of HCN
	750	T-Shaped	bend. of HC≡CH
734	735	T-Shaped	bend. of HC≡CH
	729	Linear	bend. of HCN

a) Scaling factors are assumed so as to reproduce the observed wavenumbers of monomers. b) Optimized geometrical structures are drawn in Fig. 9. c) Tentatively assigned to cyanoacetylene.

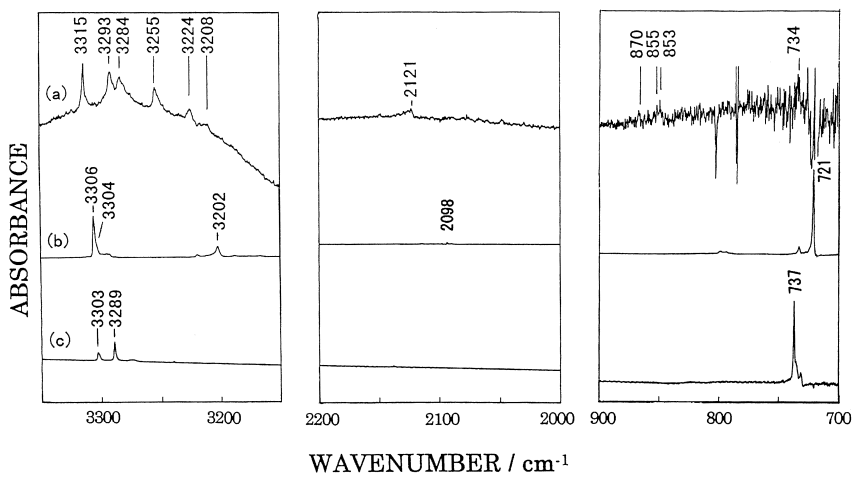

Fig. 10. Infrared spectra of HC≡CH···$(HCN)_2$ clusters in low-temperature argon matrices. (a) HC≡CH···$(HCN)_2$ clusters produced by photolysis of pyrimidine. (b) HCN/Ar = 1/1000. (c) HC≡CH/Ar = 1/1000. (Unpublished data).

tion due to collisions with the surface. In order to examine this question, we directly deposited 1,2-dichloroethane in a supersonic jet on a cold plate and measured infrared bands of the *trans* and *gauche* conformers shown in Scheme 6.[40] After confirmation that no redistribution of the conformers takes place in collision on the matrix surface, we measured infrared spectra of N_2O clusters[41] and CH_3I dimers[42] in supersonic jets, from which we could estimate the geometrical structures of the clusters by comparing the observed wavenumber shifts from monomer with the corresponding calculated values.

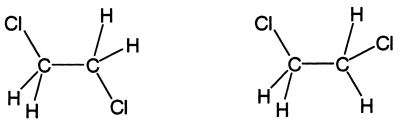

Scheme 6.

5.1 Test of Cooling Effects on Supersonic-Jet Expansion. According to Felder and Günthard, no significant conformational cooling was found for 1,2-dichloroethane.[43,44] However, their results are contrary to the fact that molecules are cooled translationally, rotationally and vibrationally by supersonic expansion. We adopted a pulsed nozzle instead of the continuous nozzle used in their experiments and avoided using a differential pumping system with a skimmer and a system of mixing with argon introduced through another nozzle. Our experimental setup is shown in Fig. 11: The distance from the nozzle to the cold CsI plate was 20 mm; the diameter of the orifice of the nozzle was 300 μm; the pulse width and the pulse interval were fixed to 169 μs and 1 Hz, respectively.

Figure 12 shows the dependence of the conformational temperature, which was derived from the absorbance ratio of *trans* and *gauche* conformers and the enthalpy difference between the two conformers, on the stagnation pressure. Despite appreciable experimental error, the temperature decreased steeply in the beginning and thereafter decreased slowly as the stagnation pressure increased. The solid line represents calculated values obtained by using an empirical equation, $T = T_0\{1 + (aP_0)^b\}^{-1}$, where T_0 and P_0 are the temperature and pressure of the sample in the reservoir, respectively. The parameters, a and b, were

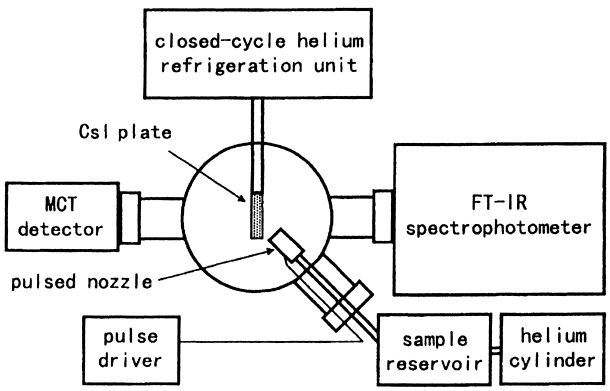

Fig. 11. Schematic figure of our experimental setup. (Transfer from *J. Mol. Struct.*, **524**, 62 (2000)).

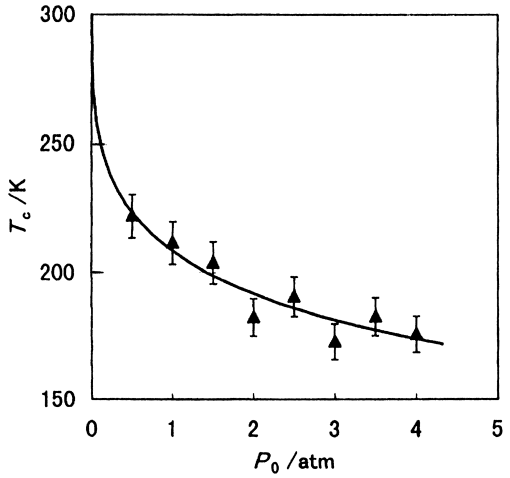

Fig. 12. Dependence of conformational temperature on stagnation pressure. Solid line represents the calculated values. (Transfer from *Chem. Phys. Lett.*, **296**, 331 (1998)).

determined by a least-squares fitting to be 0.10 ± 0.03 atm^{-1} and 0.36 ± 0.06, respectively. This equation is similar to a relationship between the translational temperature and the stagnation pressure.

The above results on the conformational change of 1,2-dichloroethane suggest that the landing of the molecules in a supersonic jet on the surface is so soft that no substantial conformational isomerization takes place. It is likely that the translational energies are dissipated into the cold plate and argon atoms behave as a cushion in this process. If this is true, direct deposition of supersonic jets should make it possible to measure infrared spectra of van der Waals clusters with a conventional FTIR spectrophotometer.

5.2 N_2O Clusters. N_2O clusters in a supersonic jet were directly isolated in a low-temperature argon matrix. As shown in Fig. 13, spectral changes were observed as the stagnation

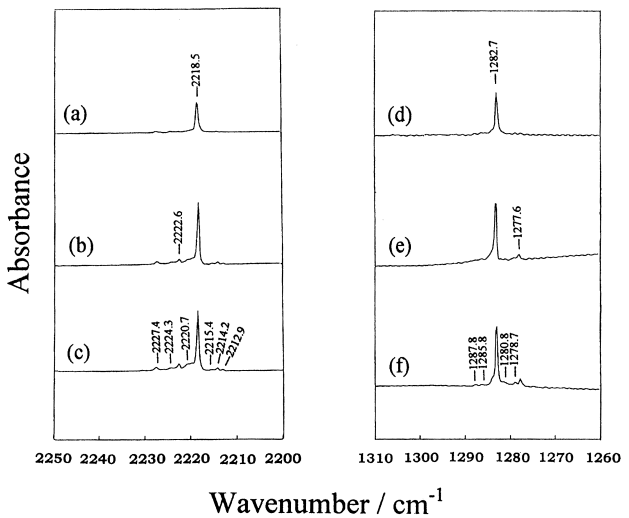

Fig. 13. Infrared spectra of N_2O clusters in low-temperature argon matrices. The stagnation pressures are (a) and (d) 1 atm; (b) and (e) 2 atm; (c) and (f) 3 atm. (Transfer from *J. Mol. Struct.*, **524**, 63 (2000)).

pressure increased. When the pushing pressure was 1 atm, only the monomer band was observed at 2218.5 cm^{-1} in the N≡N stretching region. This finding suggested that clusters were not produced in a supersonic jet, probably because of low stagnation pressure. When the pressure was 2 atm, the dimer band was observed at 2222.6 cm^{-1}. When the pressure was elevated to 3 atm, the intensities of some small bands increased a little. Similar spectral changes were observed in the N=O stretching region, where only monomer band was observed at 1282.7 cm^{-1} at the stagnation pressure of 1 atm, and the intensities of the cluster bands increased as the pressure increased.

In order to assign these bands, we performed the DFT calculation at the B3LYP/6-31+G* level. Optimized geometries for N_2O dimers and trimers are shown in Figs. 14 and 15, respectively. The calculated energy differences of N_2O dimers and trimers from monomer are summarized in Table 3. The most stable dimer is N···O antiparallel. The linear conformer is less stable than the others because the quadrupole interaction of N_2O molecules plays a more important role than the dipole moment does in this case. However, the energy differences among these dimers and trimers are so small that all the dimers and trimers are expected to exist in a supersonic jet. Our tentative assignments are shown in Table 4, where wavenumbers represent differences from monomer bands appearing at 2218.5 and 1282.7 cm^{-1}.

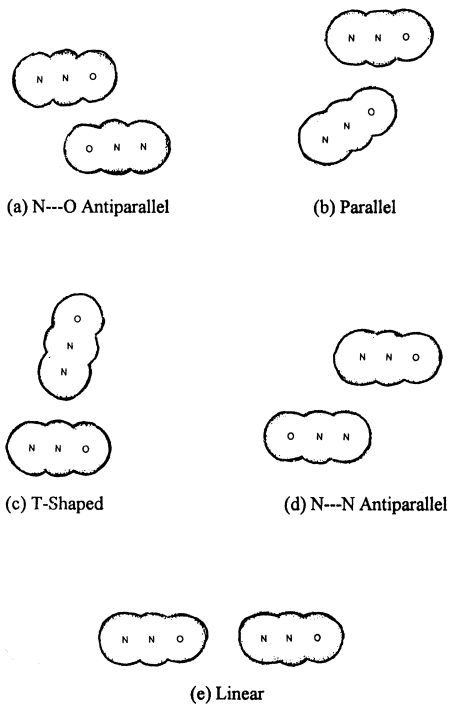

Fig. 14. Optimized geometrical structures of N_2O dimers. (Transfer from *J. Mol. Struct.*, **524**, 62 (2000)).

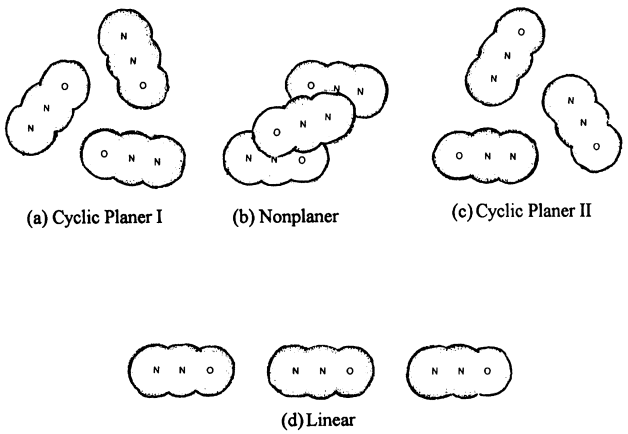

Fig. 15. Optimized geometrical structures of N_2O trimers. (Transfer from *J. Mol. Struct.*, **524**, 67 (2000)).

Table 3. Calculated Energy Differences of N_2O Clusters from Monomer (in kJ mol^{-1})

Conformer[a)]		B3LYP/6-31+G*
Dimer	N···O Antiparallel	−2.920
	Parallel	−1.857
	T-Shaped	−1.521
	N···N Antiparallel	−1.041
	Linear	−0.568
Trimer	Cyclic Planer I	−6.315
	Nonplaner	−5.974
	Cyclic Planer II	−3.855
	Linear	−1.115

a) Optimized geometrical structures are drawn in Figs. 14 and 15.

5.3 CH_3I Clusters. CH_3I in a supersonic jet was isolated in a low-temperature argon matrix. Figure 16 shows the dependence of the infrared bands for the ν_1, ν_5, ν_2, and ν_6 modes on the stagnation pressure. The intensities of dimers bands appearing around the monomer band marked with an asterisk increased as the pressure increased.

In order to assign the observed bands, we performed ab initio calculations to obtain optimized geometry and vibrational wavenumbers, where a large basis set, D95++(d, p), containing dispersion force, polarization, and diffuse functions, was used for carbon and hydrogen atoms. The double-zeta valence basis set plus the effective core potential developed by Wadt and Hay,[45] augmented by two d- and one f-type polarization functions and one s- and one p-type diffuse functions, were used for iodine atoms.

Two isomers shown in Fig. 17 were found to be stable. The head-to-tail structure, which has C_{2h} symmetry, is at a global-minimum originating from classical dipole-dipole interaction. The I–I distance, calculated to be 4.43 Å, is nearly equal to the sum of the van der Waals radii of two iodine atoms. On the other hand, the head-to-head structure, which has C_s symmetry, is 185 cm^{-1} less stable than the head-to-tail structure. The I–I distance, calculated to be 3.96 Å, is 0.34 Å shorter than the sum of van der Waals radii of two iodine atoms. This finding suggested that the two iodine atoms strongly attract each other.

The observed wavenumbers and shifts from monomer are summarized in Table 5 and compared with those obtained by the ab initio calculation. In the ν_6 mode, five bands were observed around the monomer band. Since two methyl iodide molecules in the head-to-head isomer are nonequivalent, degeneracy of this mode is broken; hence four bands appeared

Table 4. Observed and Calculated Vibrational Wavenumbers of N_2O Clusters (in cm^{-1})

Vibrational Mode	Wavenumber	Shift		Tentative Assignments
	Obsd	Obsd	Calcd	
N≡N str.	2227.4	+8.9	+7.9	Nonplaner (Trimer)?
	2224.3	+5.8	+7.7	Cyclic Planer I (Trimer)?
	2222.6	+4.1	+5.2	N···O Antiparallel
	2220.7	+2.2	+2.5	T-Shaped
	2219.7[a)]	+1.2	+1.7	Parallel
	2218.5	0	0	Monomer
	2215.4	−3.1	−1.1	N···N Antiparallel
	2214.2	−4.3	−3.7	Linear Dimer
	2212.9	−5.6	−5.6	Linear (Trimer)?
N=O str.	1287.8	+5.1	+3.5	T-Shaped, Parallel
	1285.8	+3.1	+2.5	N···N Antiparallel
	1283.9[a)]	+1.2	+1.0	T-Shaped
	1282.7	0	0	Monomer
	1280.8	−1.9	−1.7	Parallel
	1278.7	−4.0	−2.3	Linear Dimer
	1277.6	−5.1	−3.6	N···O Antiparallel

a) At shoulder of monomer bands.

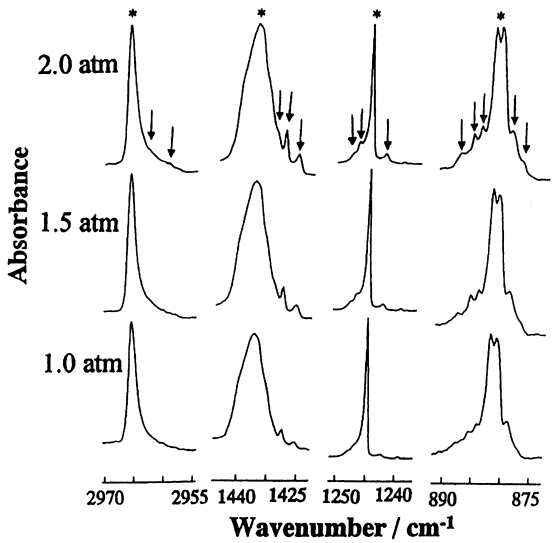

Fig. 16. Dependence of infrared bands on stagnation pressure. Mixing ratio of CH_3I/Ar is fixed to 1/2000. Symbols* and ↓ represent positions of monomer and cluster bands, respectively. Spectra are scaled so as to make the heights of the monomer bands nearly constant. (Transfer from *Chem. Phys. Lett.*, **343**, 189 (2001)).

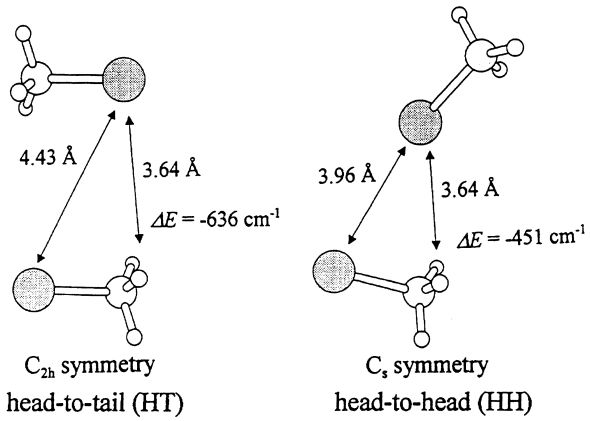

Fig. 17. Optimized geometrical structures for two isomers of $(CH_3I)_2$. ΔE denotes the BSSE-corrected dimerization energy calculated at the MP4 level. (Transfer from *Chem. Phys. Lett.*, **343**, 187 (2001)).

independently. On the other hand, two methyl iodide molecules in the head-to-tail isomer are equivalent, and hence two among four bands are infrared-inactive. The shifts calculated from the wavenumbers of monomer for the infrared-active bands are consistent with the corresponding observed values, as shown in Table 5.

All the observed bands were assigned to head-to-head or head-to-tail isomers, except for the 2959 cm^{-1} band. Thus we concluded that the head-to-head and head-to-tail isomers coexist in the argon matrices prepared by direct deposition of a supersonic jet of CH_3I.

6. Electronically Excited State of Naphthalene

Recently, time-resolved infrared spectroscopy has become a powerful technique to observe spectra of electronically excited states.[46–49] Matrix-isolation FTIR is also a powerful technique to study the lowest triplet states (T_1), because species in the excited states are stabilized in an inactive matrix at low-temperature.[50–53] The lifetime of an excited state is so long that its infrared spectrum can be measured with a conventional FTIR spectrophotometer. We measured infrared spectra of normal and deuterated naphthalene in the lowest triplet state by matrix-isolation FTIR spectroscopy.[54–56]

6.1 Matrix-Isolation Infrared Spectra. Infrared spectra of naphthalene in low-temperature argon matrices were measured by a standard technique. After the measurement, we radiated UV light on the matrix sample in order to increase the population of the T_1 state. Figure 18 shows difference spectra

Table 5. Observed and Calculated Vibrational Wavenumbers of CH_3I Dimers (in cm^{-1})

Vibrational Mode	Wavenumbers	Shift from Monomer		Tentative Assignments[a)]
	Obsd	Obsd	Calcd	
ν_1 Symmetric CH_3 Str.	2959	−7	−1.6	HH[b)]
	2963	−3	−0.8	HH
	2966	0	+1.2	HT (Monomer)
ν_5 Degenerate CH_3 Def.	1425	−7	−5.5	HT
	1427	−5	−4.8	HH
	1428	−4	−4.1, −3.7	HT, HH
	1432	0	−0.3, −0.7	HH[c)] (Monomer)
ν_2 Symmetric CH_3 Def.	1242	−3	−3.8	HH
	1245	0	0	(Monomer)
	1247	+2	+0.3	HH
	1248	+3	+2.3	HT
ν_6 Degenerate CH_3 Rock.	877	−5	−4.8	HH
	879	−3	−4.2	HH
	882	0	0	(Monomer)
	884	+2	+4.2, +4.2	HH, HT
	885	+3	+4.3	HH
	887	+5	+5.7	HT

a) HT and HH denote head-to-tail and head-to-head isomers, respectively. Optimized geometrical structures are drawn in Fig. 17. b) This band may be assigned to another dimer or trimer. c) Two bands are calculated for HH.

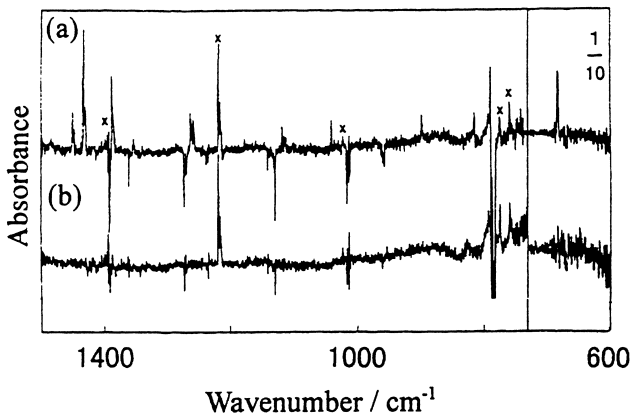

Fig. 18. Infrared spectra of naphthalene ($C_{10}H_8$) in low-temperature argon matrices. (a) A difference spectrum between those measured before and during irradiation. (b) A difference spectrum between those before and after irradiation. Bands marked by "X" are due to naphthalene radical cation. The low-wavenumber region is scaled down to one tenth. (Transfer from *J. Phys. Chem. A*, **104**, 11306 (2000))

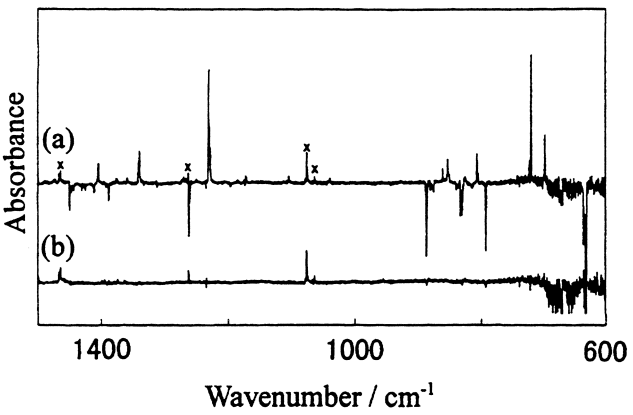

Fig. 19. Infrared spectra of naphthalene ($C_{10}D_8$) in low-temperature argon matrices. (a) A difference spectrum between those measured before and during irradiation. (b) A difference spectrum between those before and after irradiation. Bands marked by "X" are due to naphthalene radical cation. (Transfer from *J. Phys. Chem. A*, **104**, 11306 (2000)).

between the spectra measured before and during UV irradiation. The decreasing bands in Fig. 18(a) were assigned to the S_0 state, while the increasing bands were assigned to the T_1 state or a photoproduct. The increasing bands in Fig. 18(b) with symbol "X", measured before and after irradiation, were assigned to naphthalene radical cation[57–60] produced by multiphotoexcitation. By a comparison of Figs. 18(a) and (b), we found that some transient infrared bands appeared during the irradiation.

Infrared spectra of the $C_{10}D_8$ species in an argon matrix were also measured by the same experimental method. Figures 19(a) and (b) show difference spectra between the spectra measured before and during UV irradiation and between those before and after UV irradiation, respectively. By a comparison of these difference spectra, the transient infrared bands of $C_{10}D_8$ were observed. The observed wavenumbers and relative intensities are summarized in Table 6.

Table 6. Observed and Calculated Vibrational Wavenumbers (in cm^{-1}) and Relative Intensities of Infrared Active Modes of Naphthalene in the T_1 State

Mode	$C_{10}H_8$				$C_{10}D_8$			
	CIS	DFT		Obsd	CIS	DFT		Obsd
	ν	ν	Int.	ν	ν	ν	Int.	ν
$1b_{1u}$	3040	3072	64.3	3036	2244	2266	42.8	
$2b_{1u}$	3026	3059	7.7		2233	2255	1.8	
$3b_{1u}$	1427	1412	8.1	1433	1335	1347	0.2	1339
$4b_{1u}$	1382	1369	7.4	1389	1208	1203	10.1	1230
$5b_{1u}$	1238	1243	7.7	1262	1038	1023	1.0	1038
$6b_{1u}$	1019	1018	< 0.1	1041	847	844	< 0.1	853
$7b_{1u}$	784	774	6.1	790	712	703	6.9	719
$8b_{1u}$	349	345	0.1		319	316	0.1	
$1b_{2u}$	3050	3084	66.1	3059	2260	2288	37.2	
$2b_{2u}$	3025	3059	7.3		2226	2250	5.2	
$3b_{2u}$	1465	1492	0.8		1353	1461	0.4	
$4b_{2u}$	1315	1435	3.5	1450	1249	1347	0.1	
$5b_{2u}$	1130	1161	< 0.1		838	870	0.9	861
$6b_{2u}$	1054	1091	7.9	1118	833	835	7.5	806
$7b_{2u}$	777	824	< 0.1		747	770	< 0.1	
$8b_{2u}$	582	574	14.6		560	553	12.3	
$1b_{3u}$	831	789	5.7	815	698	672	7.7	696
$2b_{3u}$	705	674	108.2	682	553	526	49.3	535
$3b_{3u}$	401	382	5.0	385	342	324	8.5	
$4b_{3u}$	161	162	2.1		148	148	1.9	

6.2 Comparison between CIS and DFT Calculation. The CIS (Configuration Interaction Single) method has been used widely in recent years to calculate the vibrational wavenumbers of the electronically excited states of various simple molecules. On the other hand, fewer applications of the DFT calculation to the lowest triplet states have so far been published,[61–65] although this method was established as one of the best ways to predict vibrational wavenumbers of ground electronic states. We examined the results of the DFT and CIS calculations on the T_1 state of naphthalene by a comparison with the observed vibrational bands.

The calculated wavenumbers are summarized in Table 6, where scaling factors of 0.90 and 0.96 were used for the CIS and DFT, respectively. The relative infrared intensities obtained by the DFT method are also listed in Table 6. The calculated wavenumbers obtained by the CIS calculation are approximately equal to those obtained by the DFT calculation. However, the wavenumber of the $4b_{2u}$ mode calculated by CIS is different from that calculated by DFT by 120 cm^{-1}. It is certain that the band observed at 1450 cm^{-1} agrees well with that estimated by DFT, 1435 cm^{-1}, but not with the one estimated by CIS, 1315 cm^{-1}. Since the DFT calculation reproduced the observed wavenumbers satisfactorily for both the normal and the fully deuterated species, we concluded that the DFT calculation could predict the wavenumbers of the lowest excited triplet state of naphthalene.

Recently, time-dependent DFT method has been developed and applied to pyrazine in the T_1 state.[66,67] It is expected that TDDFT will be applicable to any electronically excited state as well as to the lowest triplet state.

7. Challenge to Detection of Oxirenes

A number of theoretical studies of oxirene, which has a highly strained three-member-ring compound containing an oxygen atom and a C=C bond, have been reported.[68–70] On the other hand, the photochemical and thermal denitrogenation of α-diazo ketones has been applied to experimental generation of oxirenes.[71–74] However, extensive matrix-isolation experiments with diazoketones failed to provide evidence for oxirene formations. We also tried to measure infrared spectra of oxirene produced by visible-light induced oxygen-atom transfer from NO_2 to alkyne.[75–77] This photoreaction is so mild that it seems likely that oxirenes exist in low-temperature argon matrices.

7.1 2-Butyne + NO_2. Samples of NO_2 and 2-butyne diluted with argon gas were co-deposited on a CsI plate. When the matrix sample was exposed to radiation from an argon ion laser-pumped CW dye laser, spectral change was observed at wavelengths as long as 610 nm. It seemed that oxygen-atom transfer from photoexcited NO_2 to the inner carbon atom of 2-butyne occurred. If the oxygen and carbon atoms of the initial reaction intermediate, 2,3-dimethyloxirene biradical, make a bond, dimethyloxirene could be generated from the biradical. However, the infrared spectrum of acetyl methyl iminoxyl radical (1-acetylethylideneamin-*N*-oxyl radical) was observed instead of dimethyloxirene; rearrangement of electron configuration in the biradical occurred immediately to yield ketocarbene, and recombination of the ketocarbene with a co-product, NO, occurred immediately to yield acetyl methyl iminoxyl radical, as shown in Scheme 7.

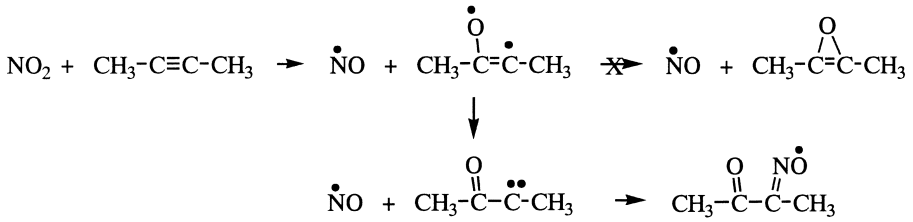

Scheme 7.

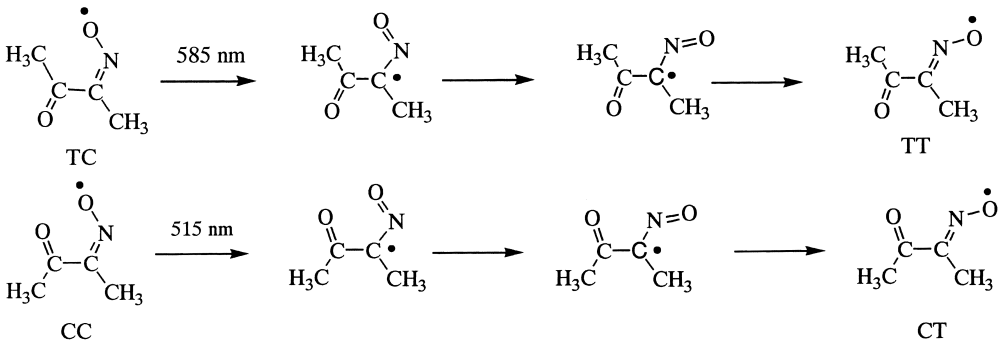

Scheme 8.

No infrared bands of iminoxyl radicals had been observed until our studies began to appear. Then, identification of this iminoxyl radical was performed by a vibrational analysis of the infrared bands including ^{18}O and ^{15}N isotope species. For example, the 1707 cm^{-1} band for the C=O stretching mode showed a shift of about 30 cm^{-1} for ^{18}O substitution. The 1560 cm^{-1} infrared band for the C=N stretching mode showed a shift of about 28 cm^{-1} for ^{15}N substitution.

Since acetyl methyl iminoxyl radical, $CH_3CO(CH_3)C{=}NO^{\bullet}$, has *trans* and *cis* conformations around the CO–CN and C=NO bonds, four conformers, TT, TC, CT, and TT, are possible. We observed infrared bands of three conformers (I_A, I_{B1}, and I_{B2}) of the iminoxyl radical generated by 585 nm irradiation. Photoisomerization from I_A to I_{B1} that occurred upon 515 nm irradiation resulted in a decrease in the intensity of I_A and an increase in that of I_{B1}, while that of I_{B2} remained unchanged. We applied the DFT calculation to acetyl methyl iminoxyl radical for prediction of the vibrational wavenumbers of four conformers to assign the observed infrared bands. The optimized geometrical structures obtained by the DFT calculations are planar for all the conformers. Conformer TT is shown to be the most stable, while CT is the least stable, probably because of the repulsion between the two lone pairs of the N and O atoms. By a comparison between the observed and calculated wavenumbers, we assigned the bands of I_A, I_{B1}, and I_{B2} to CC, CT, and TT, respectively. The overall consistency between the observed and calculated values was satisfactory, including the ^{15}N and ^{18}O isotope shifts. Then, the following reaction mechanisms for the photoisomerization around the C–N single bond, shown in Scheme 8, were proposed.

7.2 1-Phenyl-1-propyne + NO_2. Since oxirene and dimethyloxirene have four π electrons, they are antiaromatic heterocycles. On the other hand, methylphenyloxirene has 10 π electrons and belongs to the set of aromatic compounds like naphthalene. Then, the detection of methylphenyloxirene seems to be easier than those of oxirene and dimethyloxirene. However, in this visible-light induced reaction between 1-phenyl-1-propyne and NO_2, we also observed infrared spectra of iminoxyl radicals instead of methylphenyloxirene.

Two kinds of iminoxyl radicals are possible for products of the reaction between 1-phenyl-1-propyne and NO_2; one is acetyl phenyl iminoxyl radical (α-acetylbenzylideneamin-*N*-oxyl radical) and the other is benzoyl methyl iminoxyl radical (1-benzoylethylideneamin-*N*-oxyl radical). Furthermore, both *trans* and *cis* conformations around the OC–CN and C=N axes are possible as well as acetyl methyl iminoxyl radical, thus overall eight conformers are possible.

In order to identify the present iminoxyl radical, the observed vibrational wavenumbers were compared with the calculated values obtained by DFT. The optimized geometrical structures obtained are planar for all the conformers; their geometrical parameters of the molecular skeleton and relative energies are summarized in Table 7. The candidates for the iminoxyl radical are *trans–trans* acetyl phenyl iminoxyl radical (AP-TT) and *trans–trans* benzoyl methyl iminoxyl radical (BM-TT), which are the most stable conformer in each group. By a comparison of the observed wavenumber with the predicted values obtained by the DFT calculation, including ^{15}N isotope shifts, we concluded that the observed bands were assignable to AP-TT, although the relative energy of AP-TT is slightly higher than that of BM-TT.

The photoreaction mechanism (Scheme 9) was proposed to explain this complete selectivity.

The first reaction step is the oxygen-atom transfer from electronically excited NO_2 to 1-phenyl-1-propyne to produce 1-methyl-2-phenyloxirene biradical and/or 2-methyl-1-phenyloxirene biradical. The oxirene biradical immediately changes to oxirene by ring closure or to ketocarbenes by rearrangement

Table 7. Optimized Geometrical Structures (in Å or degrees) and Relative Energies (in kJ mol^{-1}) of Isomers of Iminoxyl Radical

Conformer[a)]	TT	TC	CC	CT
ΔE[b)]	−20.08	−14.38	−7.34	0.00
r(N–O)	1.227	1.228	1.225	1.222
r(C=N)	1.296	1.294	1.301	1.297
r(C–C)	1.492	1.505	1.497	1.497
r(C=O)	1.223	1.222	1.221	1.221
r(CN–CH_3)	1.505	1.503	1.505	1.511
r(CO–CH_3)	1.515	1.511	1.518	1.518
∠(C–N–O)	133.0	136.1	131.3	133.8
∠(C–C–N)	116.8	121.9	117.5	115.2
∠(C–C–O)	119.2	117.5	120.9	121.5
∠(C–CN–CH_3)	122.0	119.1	123.8	124.0
∠(C–CO–CH_3)	118.8	119.9	117.1	116.8

a) See Scheme 8. b) Relative energies.

of electrons. Since the relative energies of methylphenyloxirene and 1-benzoylethylidene are about 30 kJ mol^{-1} higher than that of α-acetylbenzylidene and the energy differences between oxirene biradicals and oxirene are about 0.2 kJ mol^{-1}, 1-benzoylethylidene is immediately isomerized to α-acetylbenzylidene. Then α-acetylbenzylideneamin-*N*-oxyl radical, AP-TT, is produced from α-acetylbenzylidene by recombination with a reactive co-product, NO.

8. Conformational Analysis

As described in the Introduction, most of the vibrational wavenumbers predicted by DFT are shown to be consistent with the corresponding observed bands within 10 cm^{-1} if a suitable scaling factor is used. Thus accurate predictions by DFT have enabled correct identification of conformers among various possibilities, no matter whether or not their spectral patterns are clearly distinguishable from one another. We determined the conformations of fundamental molecules that have some rotational axes, such as dimethylaminomethanol and 1,2-ethanediamine, by a combination of MI with DFT.[78–80]

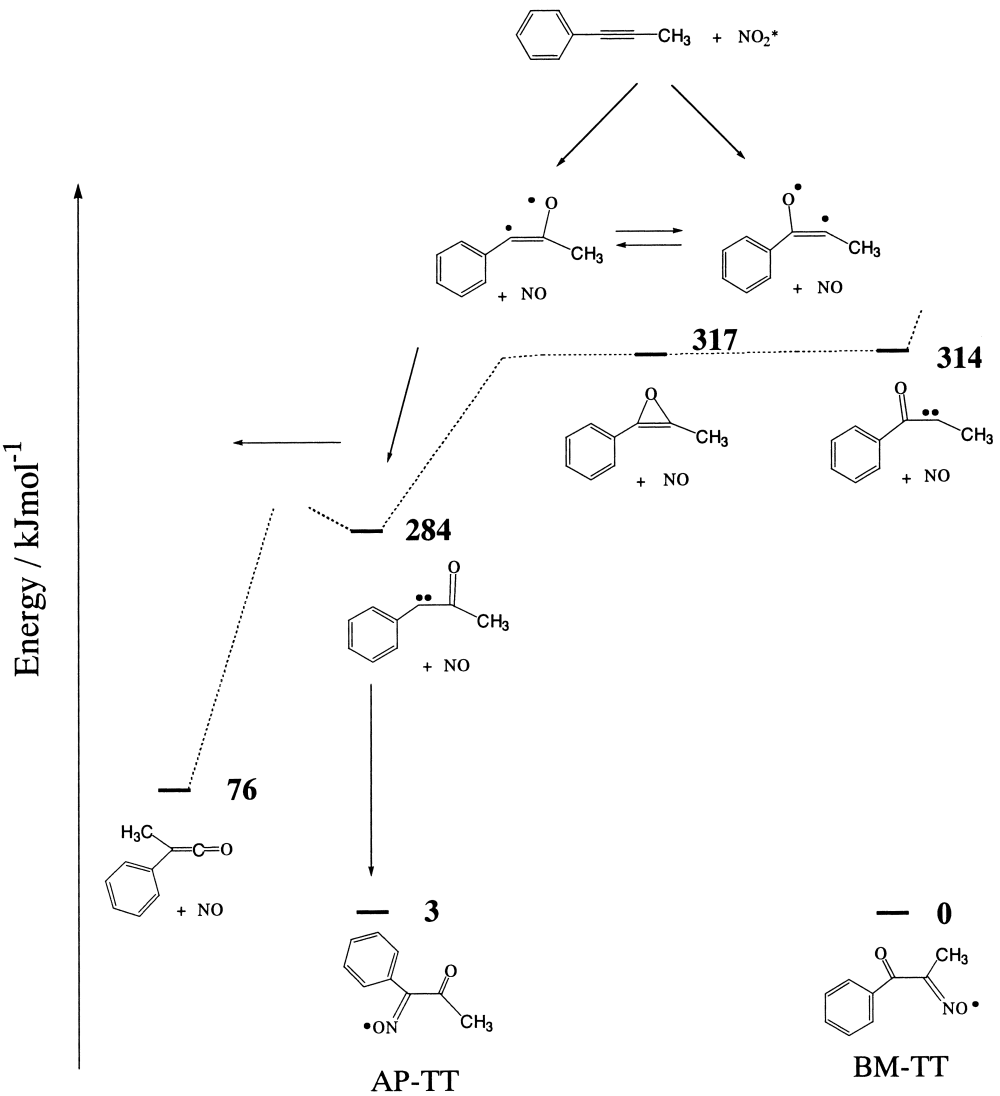

Scheme 9.

Table 8. Visible-Light Induced Bimolecular Reactions between NO_2 and Organic Compounds in Argon Matrices.

Reactants	Wavelength	Intermediates	Final Products	Ref.
$CH_2{=}CH_2 + NO_2$	< 555 nm	$^{\bullet}CH_2CH_2ONO$,	CH_3CHO, Oxirane	84, 85
$CH_3CH{=}CH_2 + NO_2$	< 595 nm	$CH_3{}^{\bullet}CHCH_2ONO$	Methyloxirane	86
trans-$CH_3CH{=}CHCH_3 + NO_2$	< 620 nm	*trans*-$CH_3{}^{\bullet}CHCH(CH_3)ONO$	*trans*-1,2-Dimethyloxirane	87
cis-$CH_3CH{=}CHCH_3 + NO_2$	< 620 nm	*cis*-$CH_3{}^{\bullet}CHCH(CH_3)ONO$	*cis*-1,2-Dimethyloxirane, $(CH_3)_2CHCHO$	88
$(CH_3)_2C{=}CH_2 + NO_2$	< 620 nm	$(CH_3)_2{}^{\bullet}CCH_2ONO$	1,1-Dimethyloxirane, $(CH_3)_2CHCHO$	89
$(CH_3)_2C{=}C(CH_3)_2 + NO_2$	< 650 nm	$(CH_3)_2{}^{\bullet}C(CH_3)_2ONO$	1,1,2,2-Tetramethyloxirane, $(CH_3)_3CCOCH_3$	90, 91
$CH_2{=}CH{-}CH{=}CH_2 + NO_2$	< 582 nm	Nitrite Radical	Oxirane, Aldehyde	92
$CH_2{=}C(CH_3){-}CH{=}CH_2 + NO_2$	< 582 nm	Nitrite Radical	Oxirane, Aldehyde	92
$CH_2{=}C(CH_3){-}C(CH_3){=}CH_2 + NO_2$	< 582 nm	Nitrite Radical	Oxirane, Aldehyde	92
$CH_2{=}C{=}CH_2 + NO_2$	< 585 nm	$CH_2{=}C(ONO)CH_2{}^{\bullet}$	Oxirane, Cyclopropanone	75
cyclopentene + NO_2	< 610 nm	Nitrite Radical	Oxirane	93, 94
cyclohexene + NO_2	< 610 nm	Nitrite Radical	Oxirane	93, 94
1,3-cyclohexadiene + NO_2	< 640 nm	Nitrite Radical	Oxirane, Benzene	95
1,4-cyclohexadiene + NO_2	< 630 nm	Nitrite Radical	Benzene	96
$HC{\equiv}CH + NO_2$	< 582 nm		$CH_2{=}C{=}O$	97, 98
$CH_3C{\equiv}CH + NO_2$	< 615 nm	Iminoxyl Radical	$CH_3C{\equiv}COH$, $CH_3CH{=}C{=}O$	97, 98
$CH_3C{\equiv}CCH_3 + NO_2$	< 610 nm	Iminoxyl Radical	$(CH_3)_2C{=}C{=}O$	75, 76
$C_6H_5C{\equiv}CCH_3 + NO_2$	< 610 nm	Iminoxyl Radical	$C_6H_5CH_3C{=}C{=}O$	77
$NH_2CH_3 + NO_2$	< 585 nm	CH_3NHOH	$CH_2{=}NH$	99
$NH(CH_3)_2 + NO_2$	< 585 nm	$(CH_3)_2NOH$	$CH_2{=}N{-}CH_3$	100
$N(CH_3)_3 + NO_2$	< 585 nm	$(CH_3)_2NCH_2{}^{\bullet}$, HONO	$(CH_3)_2NCH_2OH$	78

8.1 Dimethylaminomethanol. Recently we have studied visible-light induced bimolecular reactions between NO_2 and various organic compounds in low-temperature argon matrices.[81–100] since completely stereoselective photo-oxidation of *trans* 2-butene to oxirane was observed in 1989. These initial steps of the mild photo-oxidation can be divided into two groups: oxygen-atom transfer from NO_2 to organic compounds and hydrogen-atom elimination from organic compounds by NO_2. Infrared spectra of some new reaction intermediates such as nitrite and iminoxyl radicals were observed, as listed in Table 8. Among the final products, dimethylaminomethanol produced from trimethylamine and NO_2 was a new molecule and no spectroscopic data had been published until our studies.

Dimethylaminomethanol, $(CH_3)_2NCH_2OH$, has *gauche* and *trans* conformations around the $(CH_3)_2N{-}CH_2OH$ and $(CH_3)_2NCH_2{-}OH$ bonds, so several conformers are possible. We performed the DFT calculations to identify the observed infrared spectra; our results showed that TT, TG, and GG conformer are deemed stable among the possible conformers, as shown in Scheme 10. The energy of TG is higher than GG by only 0.77 kJ mol^{-1}, while that of TT is higher than GG by 3.89 kJ mol^{-1}.

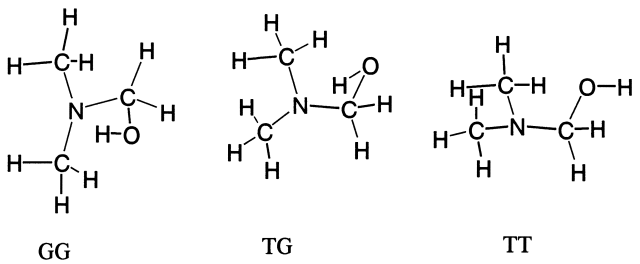

Scheme 10.

The calculated wavenumbers, relative intensities, and isotope shifts of GG and TG satisfactorily reproduced the observed values. The following reaction mechanism shown in Scheme 11 was proposed:

$$(CH_3)_3N + NO_2 \rightarrow (CH_3)_2NCH_2{}^{\bullet} + HONO \rightarrow (CH_3)_2NCH_2{}^{\bullet} + {}^{\bullet}OH + NO \rightarrow (CH_3)_2NCH_2OH + NO$$

Scheme 11.

8.2 1,2-Ethanediamine. Several stereo-chemical studies of 1,2-ethanediamine have been made. Conformational isomerism, however, has not been clarified in detail, because a large number of conformers are possible by a combination of atomic positions around three rotational axes. We observed infrared spectra of this molecule in argon matrices and determined the conformations with an aid of DFT calculation. The observed infrared bands, including $ND_2CH_2CH_2ND_2$ and $NH_2CD_2CD_2NH_2$ species, were assigned to two *gauche* ($G^+G^+G^-$ and TG^+G^-) and one *trans* (TTT) isomers. Isomerization around the central C–C axis from *gauche* to *trans* was found to occur upon infrared irradiation, as shown in Scheme 12.

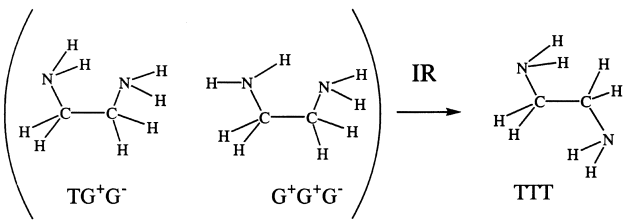

Scheme 12.

9. Summary and Perspective

The low-temperature matrix-isolation infrared spectroscopy combined with the density-functional-theory calculations has been applied to studies of species undetected in the normal experimental condition; for example, Dewar pyridine and picolines produced by UV irradiation, (2) van der Waals clusters of HCN and HC≡CH produced by photolysis of triazine or tetrazine, (3) N_2O and CH_3I clusters produced by supersonic expansion, (4) naphthalene in the electronically excited state, (5) iminoxyl radicals produced by visible-light induced reaction between NO_2 and acetylene derivatives, and (6) less stable rotational isomers of dimethylaminomethanol and 1,2-ethanediamine. The identifications for these species have been performed by comparing the observed infrared bands with the calculated spectral patterns obtained by the density-functional-theory method. Although the low-temperature matrix-isolation infrared spectroscopy was established about 50 years ago, it will be further promoted in future, combined with the development of density-functional-theory calculations.

The author sincerely thanks Prof. Kozo Kuchitsu (Josai University) for his helpful discussion and all the co-workers, especially Dr. Satoshi Kudoh, who performed the DFT calculations in our papers.

References

1 E. Whittle, D. A. Dows, and G. C. Pimentel, *J. Chem. Phys.*, **22**, 1943 (1954).
2 I. Norman and G. Porter, *Nature*, **174**, 508 (1954).
3 I. R. Dunkin, "Matrix-isolation techniques," Oxford University Press (1998).
4 A. J. Barnes, W. J. Orville-Thomas, A. Muller, and G. Gaufres, "Matrix isolation spectroscopy," D. Reidel (1981).
5 R. J. H. Clark and R. E. Hester, "Spectroscopy of matrix isolated species," John Wiley (1989).
6 D. W. Ball, Z. H. Kafafi, L. Fredin, R. H. Hauge, and J. L. Margrave, "A bibliography of matrix isolation spectroscopy," Rice University Press (1989).
7 D. W. Ochsner, D. W. Ball, and Z. H. Kafafi, "A bibliography of matrix isolation spectroscopy: 1985–1997," U. S. Department of commerce, National Technical Information Service (1998).
8 J. Labanowski and J. W. Andzelm, "Density Functional Methods in Chemistry," Springer-Verlag, New York (1991).
9 J. M. Seminario and P. Politzer, "Modern Density Functional Theory: A Tool for Chemistry," Elsevier, Amsterdam (1995).
10 C. Møller and M. S. Plesset, *Phys. Rev.*, **46**, 218 (1964).
11 P. Hohenberg and W. Kohn, *Phys. Rev.*, **136**, B864 (1964).
12 W. Kohn and L. J. Sham, *Phys. Rev.*, **140**, A1133 (1965).
13 M. W. Wong, *Chem. Phys. Lett.*, **256**, 391 (1996).
14 A. P. Scott and L. Radom, *J. Phys. Chem.*, **100**, 16502 (1996).
15 A. D. Becke, *J. Chem. Phys.*, **98**, 5648 (1993).
16 C. Lee, W. Yang, and G. R. Parr, *Phys. Rev. B*, **37**, 785 (1988).
17 J. Dewar, *Proc. R. Soc. Edinburgh*, **82** (1866–1867).
18 H. R. Ward and J. S. Winshnok, *J. Am. Chem. Soc.*, **90**, 5353 (1968).
19 H. F. Shurrell, D. W. Griffith, and J. E. Kent, *J. Raman Spectrosc.*, **2**, 147 (1974).
20 D. W. Griffith, J. E. Kent, and M. F. O'Dwyer, *Aust. J. Chem.*, **28**, 1379 (1975).
21 E. A. McNeill and F. R. Scholer, *J. Mol. Struct.*, **31**, 65 (1976).
22 D. W. Griffith and J. E. Kent, *Chem. Phys. Lett.*, **25**, 290 (1974).
23 O. L. Chapman, C. L. McIntosh, and J. Pacansky, *J. Am. Chem. Soc.*, **95**, 614 (1973).
24 D. E. Johnstone and J. R. Sodeau, *J. Phys. Chem.*, **95**, 165 (1991).
25 S. Kudoh, M. Takayanagi, and M. Nakata, *J. Photochem. Photobiol., A Chem.*, **123**, 25 (1999).
26 S. Kudoh, M. Takayanagi, and M. Nakata, *Chem. Phys. Lett.*, **308**, 403 (1999).
27 S. Kudoh, M. Takayanagi, and M. Nakata, *Chem. Phys. Lett.*, **322**, 363 (2000).
28 M. Nakata, *Anal. Sci.*, **17**, 679 (2001).
29 "GAUSSIAN 94" was employed for the calculations. M. J. Frisch, G. W. Trucks, H. B. Schlegel, P. M. W. Gill, B. G. Johnson, M. A. Robb, J. R. Cheeseman, T. A. Keith, G. A. Petersson, J. A. Montgomery, K. Raghavachari, M. A. Al-Laham, V. G. Zakrzewski, J. V. Ortiz, J. B. Foresman, J. Cioslowski, B. B. Stefanov, A. Nanayakkara, M. Challacombe, C. Y. Peng, P. Y. Ayala, W. Chen, M. W. Wong, J. L. Andres, E. S. Replogle, R. Gomperts, R. L. Martin, D. J. Fox, J. S.Binkley, D. J. Defrees, J. Baker, J. P. Stewart, M. Head-Gordon, C. Gonzalez, and J. A. Pople, Gaussian, Inc., Pittsburgh PA, 1995.
30 R. Liu, X. Zhou, and P. Pulay, *J. Phys. Chem.*, **96**, 3669 (1992).
31 J. Jones, G. B. Bacskay, J. C. Mackie, and A. Doughty, *J. Chem. Soc., Faraday Trans.*, **91**, 1587 (1995).
32 S. Kudoh, M. Takayanagi, and M. Nakata, *J. Mol. Struct.*, **413–414**, 365 (1997).
33 N. Akai, S. Kudoh, M. Takayanagi, and M. Nakata, *J. Photochem. Photobiol., A*, in press (2001).
34 S. Kudoh, M. Takayanagi, and M. Nakata, unpublished data.
35 T. Gejo, J. A. Harrison, and J. R. Huber, *J. Phys. Chem.*, **100**, 13941 (1996).
36 O. Schrems, M. Huth, H. Kollhoff, R. Wittenbech, and E. Knözinger, *Ber. Bunsen-Ges. Phys. Chem.*, **91**, 1261 (1987).
37 J. Pacansky, *J. Phys. Chem.*, **81**, 2240 (1977).
38 G. Scoles, "Atomic and Molecular Beam Methods," Vol. 1, Oxfort University Press, New York (1988).
39 G. Scoles, "Atomic and Molecular Beam Methods," Vol. 2, Oxfort University Press, New York (1992).
40 S. Kudoh, M. Takayanagi, and M. Nakata, *Chem. Phys. Lett.*, **296**, 329 (1998).
41 S. Kudoh, K. Onoda, M. Takayanagi, and M. Nakata, *J. Mol. Struct.*, **524**, 61 (2000).
42 F. Ito, T. Nakanaga, Y. Futami, S. Kudoh, M. Takayanagi, and M. Nakata, *Chem. Phys. Lett.*, **343**, 185 (2001).
43 P. Felder and Hs. H. Gunthard, *Chem. Phys. Lett.*, **66**, 283 (1979).
44 P. Felder and Hs. H. Gunthard, *Chem. Phys.*, **71**, 9 (1982).
45 W. R. Wadt and P. J. Hay, *J. Chem. Phys.*, **82**, 284 (1985).
46 H. Sun and H. Frei, *J. Phys. Chem. B*, **101**, 205 (1997).
47 M. Hashimoto and H. Hamaguchi, *J. Phys. Chem.*, **99**,

7875 (1995).
48 M. Itoh, T. Yuzawa, H. Mukaihata, and H. Hamaguchi, *Chem. Phys. Lett.*, **233**, 550 (1995).
49 M. W. Geroge, C. Kato, and H. Hamaguchi, *Chem. Lett.*, **1993**, 873.
50 B. Hoesterey, M. B. Mitchell, and W. A. Guillory, *Chem. Phys. Lett.*, **142**, 261 (1987).
51 M. B. Mitchell, W. A. Guillory, J. Michl, and J. Radziszewski, *Chem. Phys. Lett.*, **96**, 413 (1983).
52 M. B. Mitchell, G. R. Smith, and W. A. Guillory, *J. Chem. Phys.*, **75**, 44 (1981).
53 M. B. Mitchell, G. R. Smith, K. Jansen, and W. A. Guillory, *Chem. Phys. Lett.*, **63**, 475 (1979).
54 S. Kudoh, M. Takayanagi, and M. Nakata, *J. Mol. Struct.*, **475**, 253 (1999).
55 S. Kudoh, M. Takayanagi, and M. Nakata, *Fourier Transform Spectrosc.*, **2000**, 349.
56 M. Nakata, S. Kudoh, M. Takayanagi, T. Ishibashi, and C. Kato, *J. Phys. Chem.*, **104**, 11304 (2000).
57 J. Szczepanski, D. Roser, W. Personette, M. Eyring, R. Pellow, and M. Vala, *J. Phys. Chem.*, **96**, 7876 (1992).
58 F. Pauzat, D. Talbi, M. D. Miller, D. J. DeFrees, and Y. J. Ellinger, *Phys. Chem.*, **96**, 7882 (1992).
59 D. M. Hudgins, S. A. Sandford, and L. J. Allamandola, *J. Phys. Chem.*, **98**, 4243 (1994).
60 S. R. Langhoff, *J. Phys. Chem.*, **100**, 2819 (1996).
61 P. Mohandas and S. Umapathy, *J. Phys. Chem. A*, **101**, 4449 (1997).
62 B. Simard, P. I. Presunka, H. P. Loock, A. Berces, and O. Launila, *J. Chem. Phys.*, **107**, 307 (1997).
63 A. C. Stueckl, C. A. Daul, and H. U. Guedel, *J. Chem. Phys.*, **107**, 4606 (1997).
64 J. Hrusak, D. Schroeder, and S. Iwata, *J. Chem. Phys.*, **106**, 7541 (1997).
65 S. Zilberg, Y. Haas, and S. Shaik, *J. Phys. Chem.*, **99**, 16558 (1995).
66 P. Webwe and J. R. Reimers, *J. Phys. Chem. A*, **103**, 9821 (1999).
67 P. Webwe and J. R. Reimers, *J. Phys. Chem. A*, **103**, 9830 (1999).
68 G. Vacek, J. M. Galbraith, Y. Yamaguchi, H. F. Schafer, R. H. Nobes, A. P. Scott, and L. Radom, *J. Phys. Chem.*, **98**, 8660 (1994).
69 J. E. Fowler, J. M. Galbraith, G. Vacek, A. P. Scott, and H. F. Schaefer, *J. Am. Chem. Soc.*, **116**, 9311 (1994).
70 A. P. Scott, R. H. Nobes, and H. F. Schaefer, *J. Am. Chem. Soc.*, **116**, 10159 (1994).
71 C. Bachmann, T. Y. N'Guessan, F. Debu, M. Monnier, J. Pourcin, J. P. C. R. Aycard, and H. Bodot, *J. Am. Chem. Soc.*, **112**, 7488 (1990).
72 M. Torres, J. L. Bourdelande, A. Clement, and O. P. Strausz, *J. Am. Chem. Soc.*, **105**, 1698 (1983).
73 E. D. Laganis, D. S. Janik, T. J. Curphey, and D. M. Lemal, *J. Am. Chem. Soc.*, **105**, 7457 (1983).
74 P. G. Mahaffy, D. Visser, M. Torres, J. L. Bourdelande, A. Clement, and O. P. Strausz, *J. Org. Chem.*, **52**, 2680 (1987).
75 M. Nakata and H. Frei, *J. Am. Chem. Soc.*, **114**, 1363 (1992).
76 S. Kudoh, T. Uechi, M. Takayanagi, M. Nakata, and H. Frei, *Chem. Phys. Lett.*, **328**, 283 (2000).
77 T. Uechi, S. Kudoh, M. Takayanagi, and M. Nakata, *J. Phys. Chem.*, **106**, 3365 (2002).
78 S. Kudoh, T. Uechi, M. Takayanagi, M. Nakata, N. Tanaka, and K. Shibuya, *J. Mol. Struct.*, **524**, 251 (2000).
79 S. Kudoh, M. Takayanagi, M. Nakata, T. Ishibashi, and M. Tasumi, *J. Mol. Struct.*, **479**, 41 (1999).
80 N. Nagashima, S. Kudoh, M. Takayanagi, and M. Nakata, *J. Phys. Chem.*, **105**, 10832 (2001).
81 M. Nakata, "N-Centered Radicals," John Wiley & Sons Ltd. (1998).
82 M. Nakata, *J. Photochemistry*, **15**, 96 (1991).
83 M. Nakata, "Fundamentals and Advances in Photocehmistry," Gakkai Shuppan Center, Tokyo (1998).
84 M. Nakata, K. Shibuya, and H. Frei, *J. Phys. Chem.*, **94**, 8168 (1990).
85 D. J. Fitzmaurice and H. Frei, *J. Phys. Chem.*, **94**, 8168 (1990).
86 M. Nakata, Y. Somura, M. Takayanagi, N. Tanaka, K. Shibuya, T. Uchimaru, and K. Tanabe, *J. Phys. Chem.*, **100**, 15815 (1996).
87 M. Nakata and H. Frei, *J. Am. Chem. Soc.*, **111**, 5240 (1989).
88 M. Nakata and H. Frei, *J. Phys. Chem.*, **93**, 7670 (1989).
89 M. Nakata and H. Frei, *J. Chem. Soc. Jpn.*, **1989**, 1412.
90 M. Nakata, *Spectrochim. Acta*, **50**, 1455 (1994).
91 F. Blatter and H. Frei, *J. Phys. Chem.*, **97**, 3266 (1993).
92 N. Tanaka, Y. Kajii, K. Shibuya, and M. Nakata, *J. Phys. Chem.*, **97**, 7048 (1993).
93 D. J. Fitzmaurice and H. Frei, *Chem. Phys. Lett.*, **192**, 166 (1992).
94 D. J. Fitzmaurice and H. Frei, *J. Phys. Chem.*, **95**, 2652 (1991).
95 S. Kudoh, M. Takayanagi, and M. Nakata, Unpublished data.
96 N. Tanaka, M. Nakata, and K. Shibuya, *J. Photochem. Photobiol., A: Chem.*, **106**, 113 (1997).
97 J. A. Harrison and H. Frei, *J. Phys. Chem.*, **98**, 12142 (1994).
98 J. A. Harrsion and H. Frei, *J. Phys. Chem.*, **98**, 12152 (1994).
99 N. Tanaka, J. Oike, Y. Kajii, K. Shibuya, and M. Nakata, *Chem. Phys. Lett.*, **232**, 109 (1995).
100 N. Tanaka, J. Oike, K. Shibuya, and M. Nakata, *J. Phys. Chem.*, **100**, 4873 (1996).

Munetaka Nakata was born in Toyohashi, Japan, in 1953. He received his M.Sc. (1979) and Ph.D. (1982) degrees from The University of Tokyo, working under the direction of Professor K. Kuchitsu, with whom he studied electron diffraction and microwave spectroscopy. He worked as a Research Associate in the laboratory of Professor M. Tasumi at The University of Tokyo from 1981 to 1987, and then moved to Hiroshima University as a Lecturer. In 1989, he was appointed to Associate Professor of Tokyo University of Agriculture and Technology and promoted to Professor of Graduate School of BASE (Bio-Applications and Systems Engineering) at the same university in 1995. His current research interest is photo-induced dynamics of molecules and van der Waals clusters in low-temperature rare-gas matrices.